Electronic Supplementary Information – Improving the stability of hybrid perovskite $FAPbI_3$ by forming 3D/2D interface with organic spacers

Yun-Sim Kim[1], Chol-Hyok Ri[1], Yun-Hyok Kye[1], Un-Gi Jong[1], Chol-Jun Yu[1*]

[1] *Computational Materials Design (CMD), Faculty of Materials Science, Kim Il Sung University, Ryongnam-Dong, Taesong District, Pyongyang, Democratic People's Republic of Korea.*

June 14, 2022

Computational details

Structural optimizations and electronic structure calculations were performed using the pseudopotential plane wave method as implemented in the Quantum ESPRESSO package [1]. We used the ultrasoft pseudopotentials for relevant atoms, and the vdW-DF-ob86 [2] and Perdew-Burke-Ernzerhof (PBE) [6] functionals within the generalized gradient approximation (GGA) for the exchange-correlation (XC) interaction between the valence electrons. The plane-wave kinetic cutoff energies were set to be 70 and 600 Ry for wave functions and electron densities, respectively. The special *k*-point meshes were $8 \times 8 \times 8$ and $4 \times 4 \times 1$ for bulk and interface models, respectively. All of the atom positions were relaxed until the atomic forces converged to 5×10^{-5} Ry/Bohr.

We considered the effect of FA cation orientation of the 3D part on the structural and electronic properties. We performed structural optimizations of FAPI unit cells with three different initial FA orientations, distinguished by orientation of line from C atom to the middle point between two N atoms along the <100>, <110> and <111> directions. After optimization process, it turned out that the <100> orientation structure was not formed and transformed to the <110> orientation. Then we present the structural and electronic properties of FAPI bulk obtained using the unit cell with the <110> and <111> orientation of FA cation as shown in Fig. S8. We found that the unit cell with the <110> orientation has the lattice constant of 6.37 Å and band gap of 1.48 eV, which are in good agreement with the experimental values of 6.35 Å and 1.45 eV. Meanwhile, for the case of <111> orientation, the lattice constant and band gap were obtained to be 6.40 Å and 1.52 eV, respectively, both of which are more over the corresponding experimental values compared with the <110> case. Moreover, the total energy of the unit cell with the <110> orientation was 0.04 eV lower than that with the <111> one, indicating that the <110> orientation in FAPI is energetically more stable than the <111> orientation. Through the present work, we therefore employed the <110> orientation. In spite of the fact revealed from the bulk calculation, we further considered the different direction of spontaneous polarization field of FA in the 3D part on the electronic structure of interface. As a typical example, we constructed the two different FAPI-AN interface systems with <110> FA orientation and the inverse direction, and calculated the band structures, as shown in Fig S9. We found that the two band gaps were almost identical as 1.75 eV, indicating that the different directions of spontaneous polarization field of FA cation in the 3D part have not much effect on electronic structure of the interface system.

For the case of hybrid iodide perovskites such as MAPI and FAPI, the PBE functional was found to give band gaps agreed well with the experimental values, due to the fortuitous error cancellation between the underestimation of PBE and overestimation by ignoring the spin-orbit (SOC) coupling effect. We calculated the band structure of FAPI bulk with both PBE and hybrid HSE06 [12] functionals with and without SOC effect, as shown in Fig. S10. It turned out that PBE could give the band gap of 1.48 eV in excellent agreement with the experimental value of 1.45 eV, HSE06 greatly overestimated the band gap as 2.01 eV, and both of PBE+SOC and HSE06+SOC severely underestimated the band gap as 0.23 eV and 0.76 eV, respectively. For the cases of including SOC effect, the underestimation was mainly attributed to the down-shift of the lowest conduction band, namely Rashba effect.

The activation barriers for water diffusion were estimated by applying the nudged elastic band (NEB) method [3, 4] in connection with the SIESTA package [5], where the double-ζ polarization (DZP) basis sets were used. For the XC functional, we used the PBE fashion with the van der Waals (vdW) dispersion correction [7], as confirmed to give reliable results for the interface systems in our previous works [8, 9]. During the NEB calculation, eight images were generated along the migration path between the initial and final states. The lowest three atomic layers were fixed to their initial positions and the rests were allowed to relax until the atomic forces were less than 0.03 eV/Å.

*Corresponding author: Chol-Jun Yu, Email: cj.yu@ryongnamsan.edu.kp

The binding strength between the interface layers, the binding energy between the 3D perovskite combined with one OS layer (3D-OS1) and the 2D perovskite with one OS layer (2D-OS1) was calculated by using the following equation,

$$E_b = E_{\text{int}} - E_{\text{3D-OS1}} - E_{\text{2D-OS1}}, \tag{1}$$

using the DFT total energies of the interface system (int) and separate subsystems. We also evaluated the binding energies between the 3D part and the 2D part combined with two OS layers (2D-OS2), and between the 3D part combined with two OS layers (3D-OS2) and the 2D part by using the following equations,

$$E_{b1} = E_{\text{int}} - E_{\text{3D}} - E_{\text{2D-OS2}} \tag{2}$$

$$E_{b2} = E_{\text{int}} - E_{\text{3D-OS2}} - E_{\text{2D}} \tag{3}$$

The interlayer spacing distance d_{int} was measured as the distance between the top PbI_2 layer of the 3D part and that of the 2D part. In the formation of these interface systems, the OS iodide molecules such as BAI and PEAI infiltrates into the 3D surface and bisect the perovskite into 2D domains [10, 11]. Thus, the formation energy per area of 3D/2D interface was calculated by using the following equation,

$$E_f = \frac{1}{A}\left(E_{\text{int}} - 4E^{\text{bulk}}_{\text{FAPI}} - 2E_{\text{PEAI/BAI/ANI}}\right) \tag{4}$$

where A is the interfacial area, and $E^{\text{bulk}}_{\text{FAPI}}$ and $E_{\text{PEAI/BAI/ANI}}$ are the total energies of the unit cell of bulk FAPI and isolated BAI or PEAI or ANI single molecule (see Fig. S2), respectively.

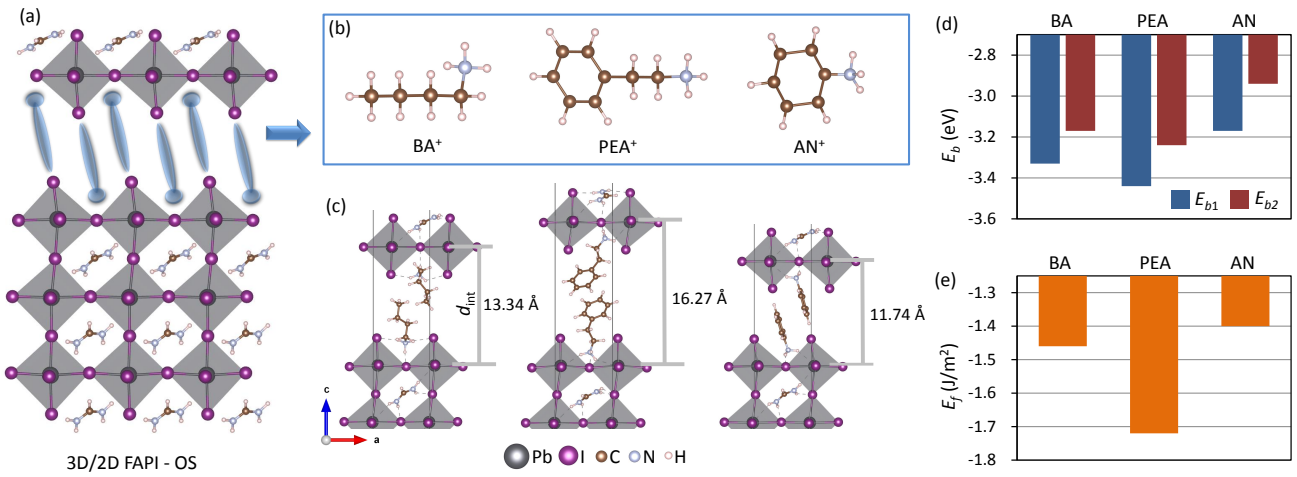

Fig. S1. (a) Schematic representation of 3D/2D interface based on formamidinium lead iodide $FAPbI_3$ (FAPI) and different organic spacer (OS) ammonium cations. (b) Ball-and-stick view of optimized structures for the three different isolated OS cations; butylammonium (BA^+), phenylethylammonium (PEA^+) and anilinium (AN^+). (c) Polyhedral and ball-and-stick view of optimized structures for the FAPI-based 3D/2D interfaces with three different OS cations, where the interface spacing distance d_{int} is defined as the distance between the PbI_2 layers of 3D and 2D parts. Dashed lines represent the hydrogen bond between I and H atoms. (d) Calculated interface binding energies between the 3D and 2D-OS2 parts (E_{b1}), and 3D-OS2 and 2D parts (E_{b2}). (e) Calculated formation energies per area for the interfaces from bulk FAPI and ligand iodide molecules like BAI, PEAI and ANI.

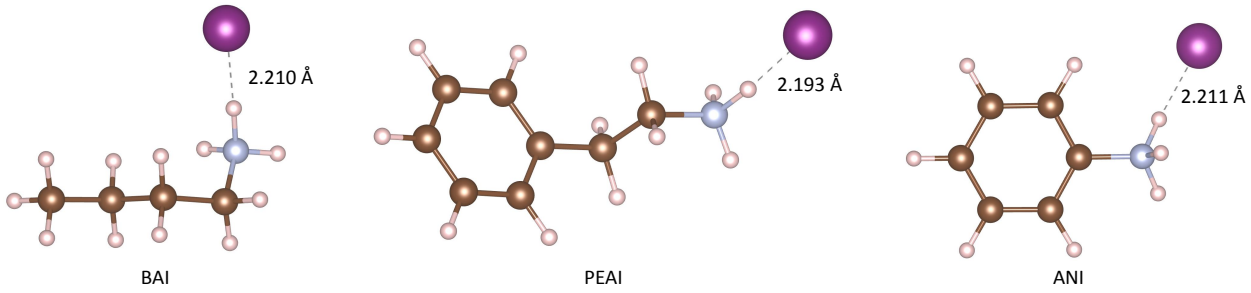

Fig. S2. Ball-and-stick view of optimized molecular structures of ammonium iodides including BAI, PEAI and ANI. Bond length between I and H atoms are displayed.

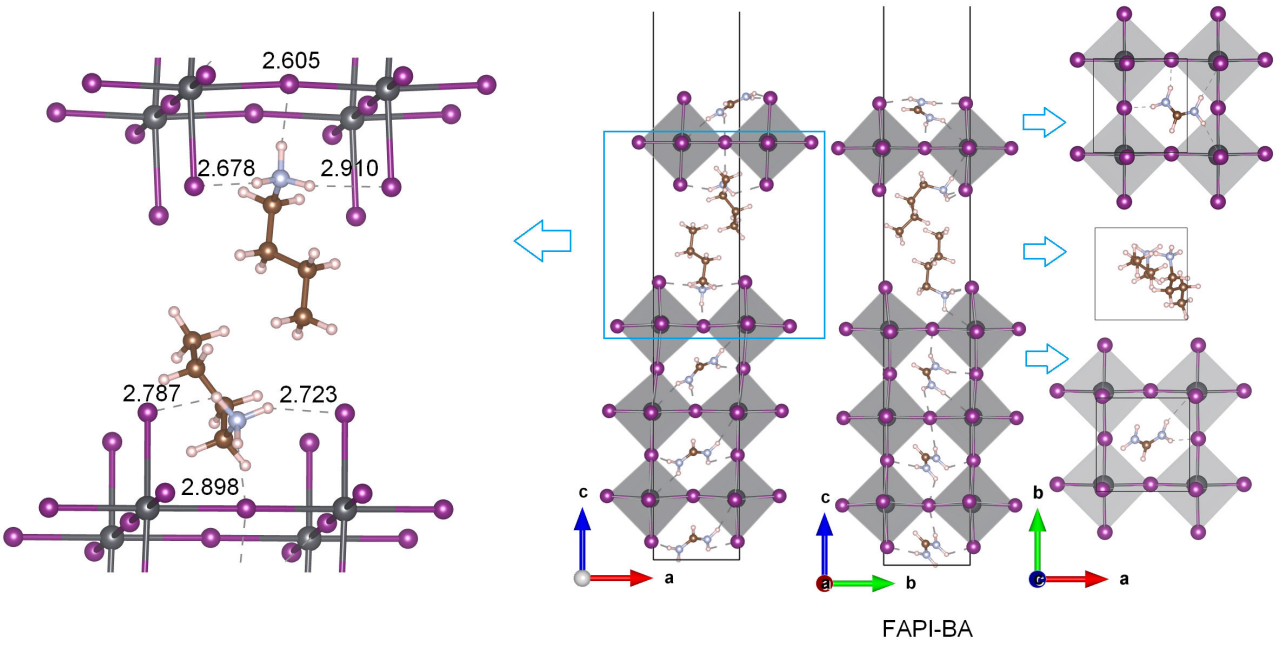

Fig. S3. Detailed atomic structure of FAPI-BA 3D/2D interface. The hydrogen bond lengths between the H and I atoms are displayed.

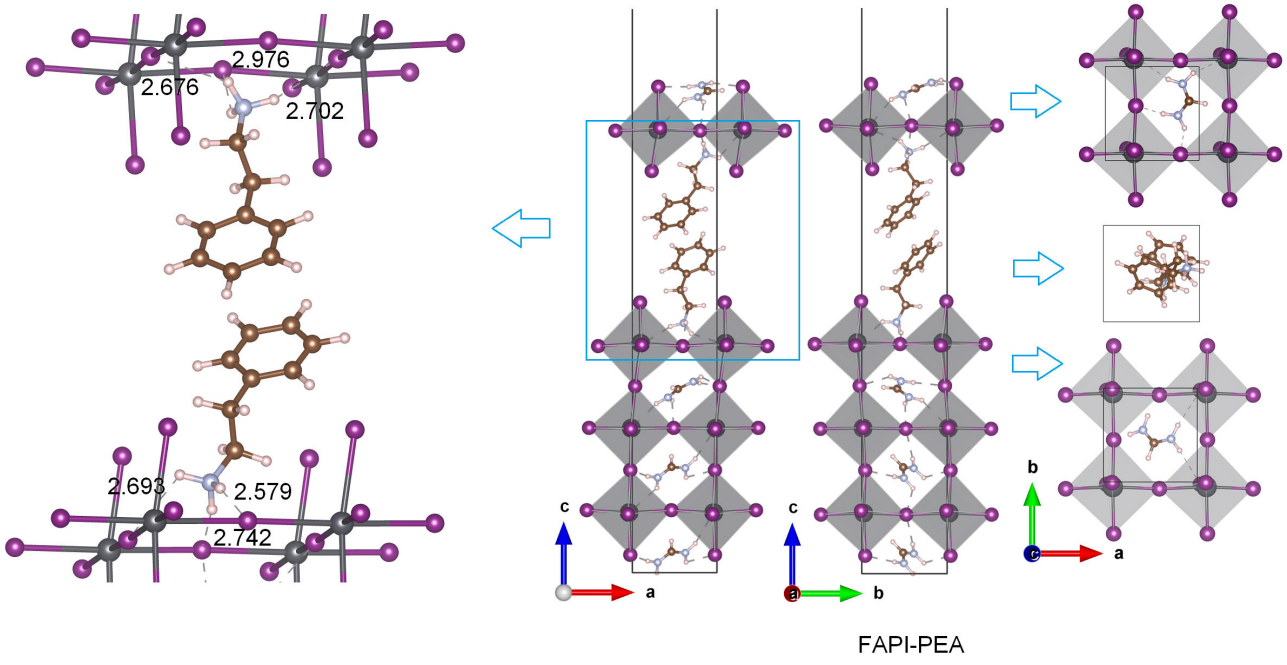

Fig. S4. Detailed atomic structure of FAPI-PEA 3D/2D interface. The hydrogen bond lengths between the H and I atoms are displayed.

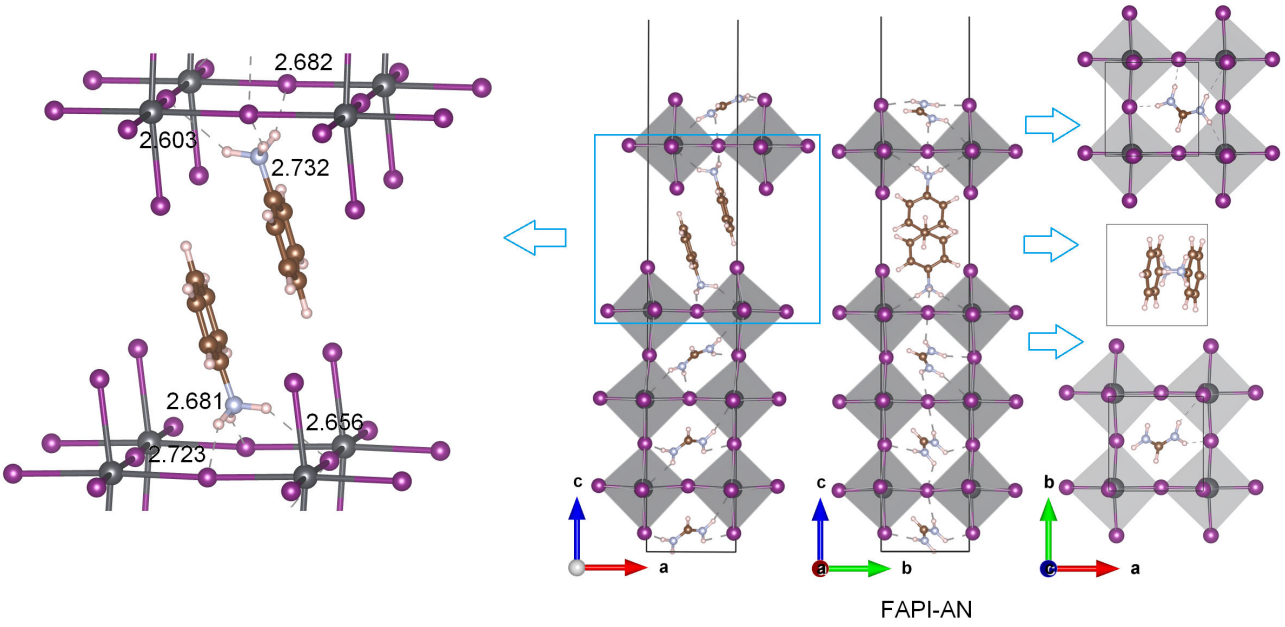

Fig. S5. Detailed atomic structure of FAPI-AN 3D/2D interface. The hydrogen bond lengths between the H and I atoms are displayed.

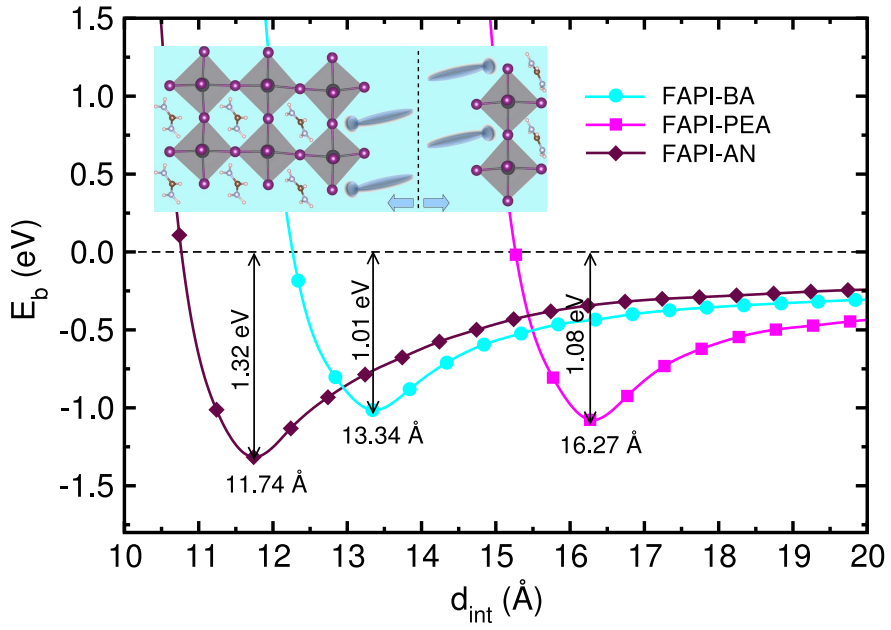

Fig. S6. Binding energy E_b as a function of interface spacing distance d_{int} for OS-bridged FAPI 3D/2D interfaces with OS being BA, PEA and AN. Equilibrium distance and the corresponding binding energy are presented. Inset shows schematic view for separating the interface system into the two parts.

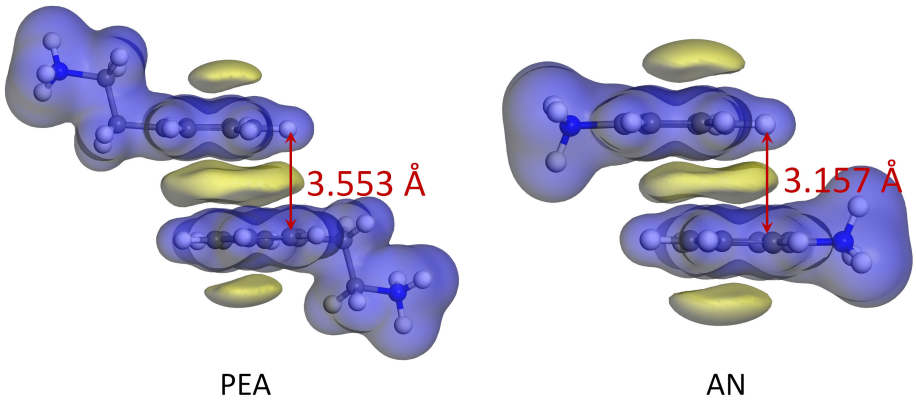

Fig. S7. Isosurface view of electrostatic potential at the value of 0.5 for PEA and AN. Yellow (blue) color represents the positive (negative) potential.

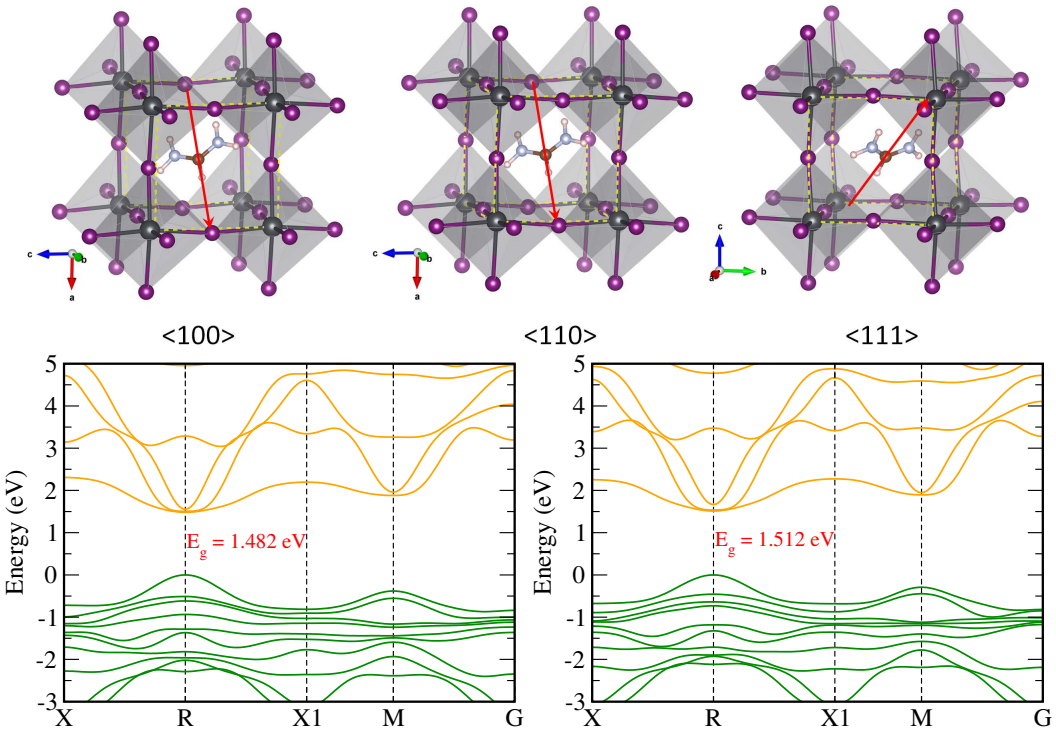

Fig. S8. Polyhedral view of optimized FAPI unit cells with different FA orientations of <100>, <110> and <111> (top panel), and band structures in <110> (left) and <111> (right) orientations (bottom panel).

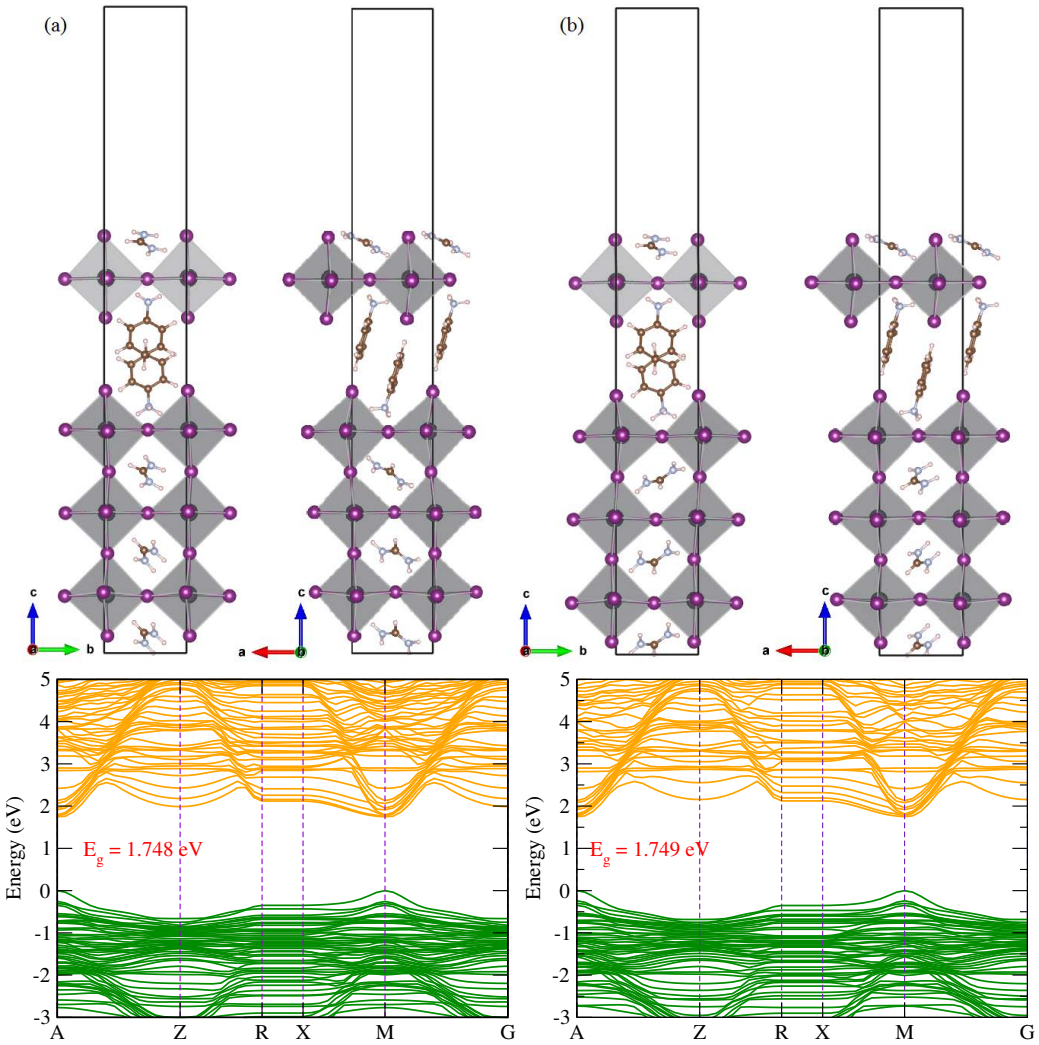

Fig. S9. Polyhedral view of optimized structures for the FAPI-AN 3D/2D interfaces with (a) <110> FA orientation and (b) inverse direction (top panel), and their electronic band structures (bottom panel).

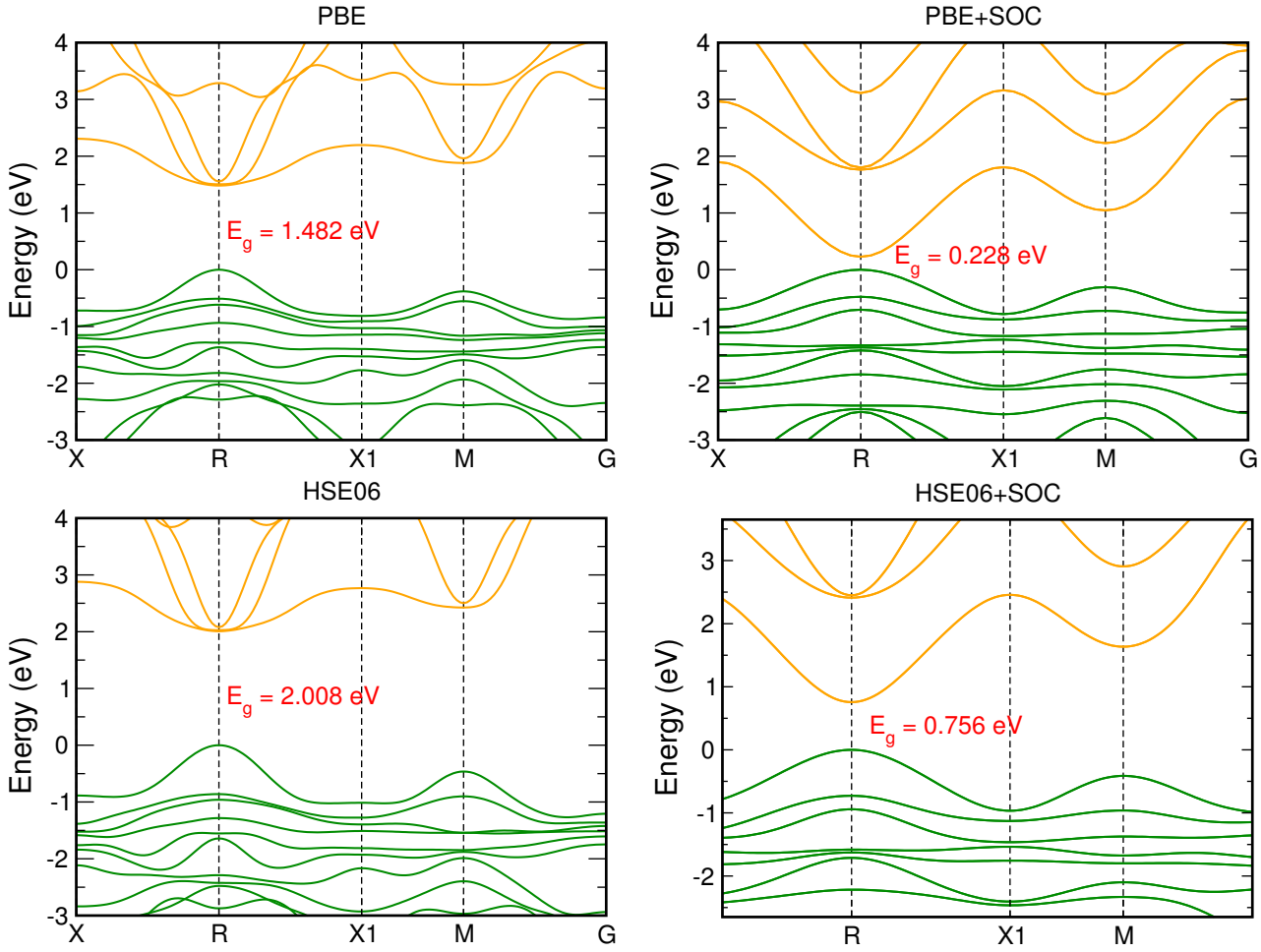

Fig. S10. Electronic band structure for bulk FAPI obtained by using PBE (top panel) and HSE06 exchange-correlation functional (bottom panel) without (left) and with (right) including spin-orbit coupling (SOC) effect. The Fermi level is set to zero, and the band gap is displayed.

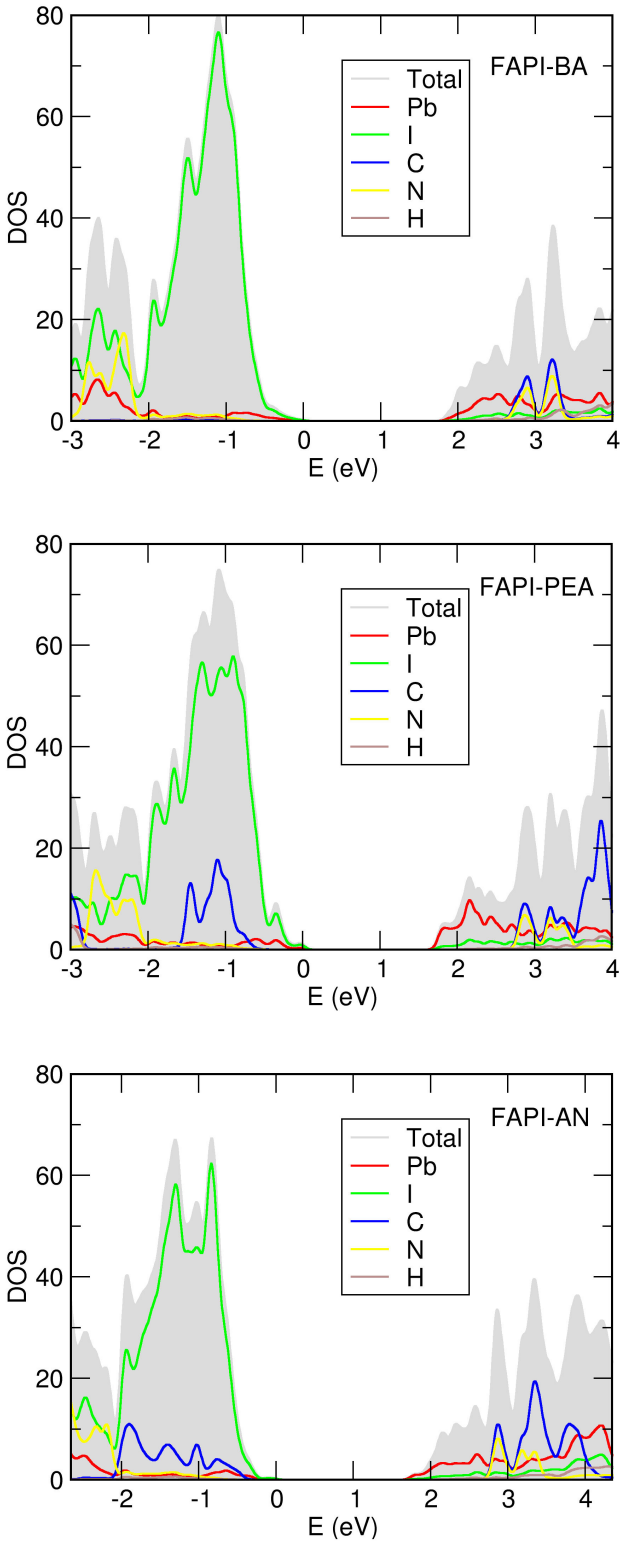

Fig. S11. Atomic resolved DOS in the interface systems with different organic spacer cations employed in this work; FAPI-BA, FAPI-PEA and FAPI-AN.

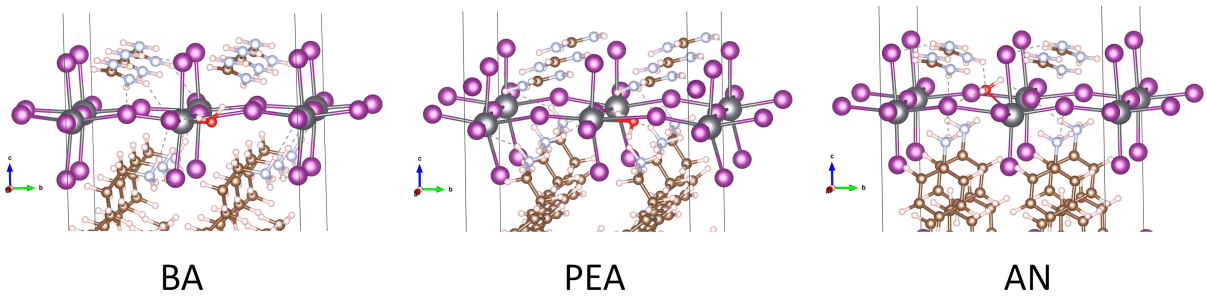

Fig. S12. Detailed atomic structures of 3D/2D FAPI-OS interface systems (OS = BA, PEA, AN) at the first transition state T1.

References

[1] P. Giannozzi, S. Baroni, N. Bonini, M. Calandra, R. Car, C. Cavazzoni,d D. Ceresoli, G. L. Chiarotti, M. Cococcioni, I. Dabo, A. Dal Corso, S. de Gironcoli, S. Fabris, G. Fratesi, R. Gebauer, U. Gerstmann, C. Gougoussis, A. Kokalj, M. Lazzeri, L. Martin-Samos, N. Marzari, F. Mauri, R. Mazzarello, S. Paolini, A. Pasquarello, L. Paulatto, C. Sbraccia, S. Scandolo, G. Sclauzero,A. P. Seitsonen, A. Smogunov, P. Umari and R. M. Wentzcovitch, *J. Solid State Chem.* 2003, **173**, 189–195.

[2] J. Klimeš, D. R. Bowler and A. Michaelides, *Phys. Rev. B: Condens. Matter Mater. Phys.*, 2011, **83**, 195131.

[3] G. Henkelman, B. P. Uberuaga and H. Jónsson, *J. Chem. Phys.*, 2000, **113**, 9901–9904.

[4] G. Henkelman and H. Jónsson, *J. Chem. Phys.*, 2000, **113**, 9978–9985.

[5] J. M. Soler, E. Artacho, J. D. Gale, A. García, J. Junquera, P. Ordejón and D. Sánchez-Portal, *J. Phys: Condens. Matter*, 2002, **14**, 2745.

[6] J. P. Perdew, K. Burke and M. Ernzerhof, *Phys. Rev. Lett.*, 1996, **77**, 3865.

[7] S. Grimme, *J. Comput. Chem.*, 2006, **27**, 1787–1799.

[8] C.-J. Yu, Y.-H. Kye, U.-G. Jong, K.-C. Ri, S.-H. Choe, J.-S. Kim, S.-G. Ko, G.-I. Ryu and B. Kim, *ACS Appl. Mater. Interfaces*, 2020, **12**, 1858–1866.

[9] Y.-S. Kim, C.-H. Ri, U.-H. Ko, Y.-H. Kye, U.-G. Jong and C.-J. Yu, *ACS Appl. Mater. Interfaces*, 2021, **13**, 14679–14687.

[10] A. H. Proppe, A. Johnston, S. Teale, A. Mahata, R. Quintero-Bermudez, E. H. Jung, L. Grater, T. Cui, T. Filleter, C.-Y. Kim, S. O. Kelley, F. De Angelis and E. H. Sargent, *Nat. Commun.*, 2021, **12**, 3472.

[11] M. A. Hope, T. Nakamura, P. Ahlawat, A. Mishra, M. Cordova, F. Jahanbakhshi, M. Mladenović, R. Runjhun, L. Merten, A. Hinderhofer, B. I. Carlsen, D. J. Kubicki, R. Gershoni-Poranne, T. Schneeberger, L. C. Carbone, Y. Liu, S. M. Zakeeruddin, J. Lewinski, A. Hagfeldt, F. Schreiber, U. Rothlisberger, M. Grätzel, J. V. Milić and L. Emsley, *J. Am. Chem. Soc.*, 2021, **143**, 1529–1538.

[12] J. Heyd, G. E. Scuseria, M. Ernzerhof, *J. Chem. Phys.*, 2003, **118**, 8207–8215.